Analyzing the Role of Topography in NO_2 Dispersion: Evidence from the 2021 Manavgat Forest Fire

Hatice Atalay[1,*], A. Filiz Sunar[2], Adalet Dervişoğlu[2]

[1]Izmir Katip Celebi University, Faculty of Engineering and Architecture, Department of Geomatics Engineering, 35620, Izmir, Türkiye, hatice.atalay@ikc.edu.tr
[2]Istanbul Technical University, Faculty of Civil Engineering, Department of Geomatics Engineering, 34469, Istanbul, Türkiye, fsunar@itu.edu.tr, adervisoglu@itu.edu.tr

Keywords: Forest Fires, NO_2 Pollution, Topography, Univariate Moran's I, Spatial Autocorrelation

Abstract

Nitrogen dioxide (NO_2), a major non-greenhouse gas, significantly impacts air quality and human health, particularly in regions affected by large-scale forest fires. The subsequent dispersion of NO_2 plumes is critically influenced by atmospheric conditions and underlying terrain, yet the specific role of topography remains under-explored, particularly in post-fire scenarios. This preliminary study investigates the influence of topographic features on NO_2 dispersion following the major 2021 Manavgat forest fire in Türkiye, utilizing satellite-derived NO_2 concentrations from Sentinel-5P TROPOMI observed during 28th July - 4 August 2021. Topographic variables—elevation, slope, and aspect—were derived from NASA's SRTM Digital Elevation Model (DEM - 30 m) to characterize the complex terrain. Univariate (UV) Moran's I was employed to evaluate the spatial autocorrelation of NO_2 concentrations, assessing patterns of clustering or dispersion and their relationship with these terrain variables. Results revealed significant positive spatial autocorrelation, indicating that higher NO_2 concentrations preferentially accumulated in lower elevations and areas with gentler slopes, while the influence of aspect appeared more variable. This suggests that topographic features acted as constraints, potentially trapping the plume and enhancing gas retention near the surface in valleys and flatter regions. These initial findings contribute to a deeper understanding of terrain-atmosphere interactions governing pollutant behavior in post-fire environments and highlight the importance of incorporating topographic parameters into localized air quality monitoring and exposure assessment frameworks.

1. Introduction

Forest fires represent significant natural disturbances impacting terrestrial ecosystems globally, particularly in Mediterranean regions prone to hot, dry summers (Pausas and Fernández-Muñoz, 2012). Beyond devastating vegetation and causing biodiversity loss, these events trigger substantial emissions of atmospheric pollutants through intense biomass combustion (Andreae and Merlet, 2001). Among these emissions, NO_2 is a prominent non-greenhouse gas pollutant with considerable impacts on environmental quality and human health (Wiedinmyer et al., 2006; Kampa and Castanas, 2008; Jaffe et al., 2020). As a short-lived reactive gas, NO_2 plays a crucial role in the formation of tropospheric ozone and secondary aerosols like fine particulate matter ($PM_{2.5}$), thereby further degrading air quality, especially in fire-affected areas (Jaffe and Wigder, 2012; Val Martin et al., 2012).

The concentration and distribution of NO_2 following a wildfire are influenced by multiple factors, including fire characteristics (e.g., intensity, size, fuel type) and prevailing meteorological conditions such as wind speed, atmospheric stability, and boundary layer height (Wiedinmyer et al., 2006; Jaffe et al., 2020). However, topography often acts as a critical, yet sometimes underappreciated, determinant of pollutant dispersion and accumulation patterns (Whiteman, 2000). Terrain features like elevation, slope, and aspect modulate local airflow, influence the formation and persistence of thermal inversions, and can create physical barriers or channels that either enhance pollutant trapping or facilitate dispersion in complex landscapes such as valleys or mountain ranges (Zhang et al., 2018). Specifically, elevation affects atmospheric pressure and temperature gradients influencing vertical mixing; slope impacts near-surface wind dynamics and turbulence; and aspect regulates solar radiation, thereby influencing surface temperature, fuel moisture, and local atmospheric stability, which collectively affect both fire behavior and subsequent pollutant transport (Dillon et.al., 2011; D'Andrea et al., 2016).

The 2021 Manavgat forest fires, among the most destructive wildfires recorded in Türkiye in recent decades, represent a significant case for examining the relationship between post-fire NO_2 distribution and topographic variability. Initiated almost simultaneously at multiple points within the Manavgat district on July 28, 2021, these fires coincided with a period of increased surface air temperatures and a prolonged heatwave that intensified fire behavior (Acar and Gonencgil, 2023). The rapid spread of the fires was further accelerated by extreme weather conditions and attributed to several causes, including human negligence and possible arson. The event resulted in the release of significant amounts of NO_2 and other trace gases and provided a unique opportunity to assess how emissions interact with the complex topography. Specifically, it allows for the investigation of how the region's complex structure may have influenced the transport and accumulation of pollutants, how topographic features may have redirected airflow by altering wind speed and direction, and whether they facilitated pollutant accumulation in topographically enclosed areas (Rotach and Zardi, 2007; Soler et al., 2011).

Advances in remote sensing and spatial analysis have greatly enhanced our ability to monitor and model atmospheric composition over complex terrains. Earth observation instruments, notably the Sentinel-5P TROPOMI (Tropospheric Monitoring Instrument) sensor, provide high spatial resolution measurements of atmospheric NO_2, enabling detailed assessments of fire-induced pollution plumes (Griffin

et al., 2021; Veefkind et al., 2007). Concurrently, DEMs, such as NASA's SRTM dataset, allow for the precise derivation of terrain metrics essential for environmental modeling and understanding landscape influences (Farr et al., 2007).

Understanding the spatial dependencies between pollutant concentrations and landscape features requires appropriate analytical tools. Given that terrain characteristics can significantly impact pollutant dispersion, leading to non-random spatial patterns, spatial statistical methods are essential. This study utilizes Moran's I, a key measure of spatial autocorrelation, to investigate these patterns (Moran, 1948; Goodchild, 1986; Atalay et al., 2025). Moran's I quantifies whether the observed spatial distribution of a variable, such as NO_2 concentration, exhibits clustering (high values near high values, low values near low values), dispersion (high values near low values), or spatial randomness. Specifically, UV Moran's I is employed to assess the spatial autocorrelation inherent within the NO_2 concentration data captured during the fire event itself (Anselin, 1995; Griffith, 2003; Atalay et al., 2025). Using this approach, it can be statistically tested whether the observed NO_2 distribution significantly deviates from spatial randomness. Detecting significant spatial clustering (a positive Moran's I) would lend support to the hypothesis that underlying factors, potentially including topographic features like valleys acting as traps or slopes influencing local airflows, are systematically structuring the NO_2 distribution rather than it being randomly scattered. Therefore, the primary objective of this research is to apply UV Moran's I to satellite-derived NO_2 data from the 2021 Manavgat wildfires to quantify the degree of spatial autocorrelation. Through the analysis of these spatial patterns, the study aims to provide an quantitative insights into how complex terrain features may have influenced the accumulation and dispersion of NO_2 during this major fire event, ultimately contributing to a better understanding of pollutant dynamics in fire-prone, topographically diverse regions.

2. Study Area and Data

2.1 Study Area

This study focuses on the Manavgat district, situated in the southern Mediterranean region of Türkiye (Figure 1). The region experiences a typical Mediterranean climate characterized by hot and arid summers, making it prone to wildfires. Reflecting this vulnerability, Manavgat was among the areas most severely affected during the extensive 2021 wildfire season. The fires resulted in a total burned area of approximately 54,8 ha, primarily within Manavgat but also extending into the adjacent districts of Ibradı and Akseki. In this fire-affected region, there are three large reservoirs - Naras, Manavgat and Oymapinar - which are crucial water sources for firefighting operations (Atalay et al., 2025). Ecologically, the area belongs to the Mediterranean forest biome, dominated by fire-prone coniferous species such as Black Pine (*Pinus nigra*) and Calabrian Pine (*Pinus brutia*).

Critically for this research, the Manavgat region exhibits significant topographic variability. Elevation ranges from 2 m near the coast to 1657 m in the mountainous interior (mean: 396 m), while slope angles vary widely from nearly flat (0°) to very steep (up to 80°, mean: 15°). Specifically, the terrain transitions from low-lying coastal plains near sea level in the south to mountainous regions exceeding 1000 meters in elevation toward the north and northeast. The central and eastern portions of the area display particularly steep elevation gradients, featuring deeply incised valleys and fragmented hill systems (Figure 2). This complex and rugged terrain, combined with the occurrence of a major fire event generating substantial NO_2 emissions, makes the Manavgat district a particularly suitable location for investigating the role of topography in influencing atmospheric pollutant dispersion.

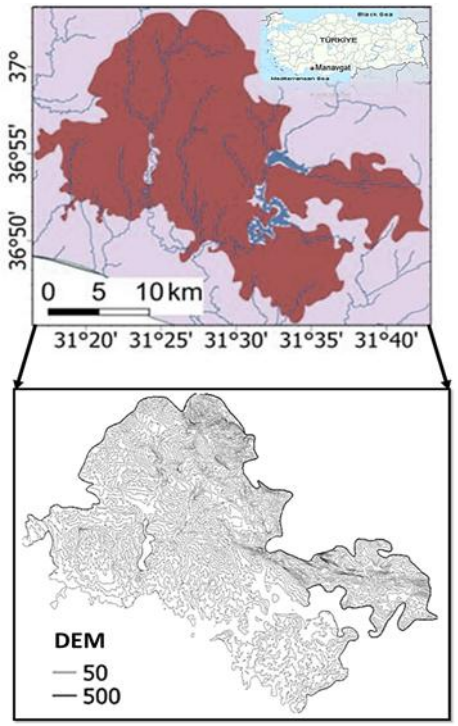

Figure 1. Study area. (Top) Map showing the location of Manavgat within Türkiye. (Bottom) Digital Elevation Model of the Manavgat fire-affected zone.

2.2. Data

2.2.1 NO_2 Concentration Data

Tropospheric NO_2 vertical column consantrations were obtained from the Sentinel-5P TROPOMI sensor. TROPOMI provides daily global observations with a nominal spatial resolution of approximately 3.5 × 5.5 km at nadir, suitable for monitoring pollution plumes from large events (Ialongo et al., 2020; Veefkind et al., 2012). To specifically capture the impact of the fire on atmospheric composition during its most intense phase, satellite data corresponding to the period of peak fire activity (primarily July–August 2021) were selected for this study. These data were then temporally organized to generate representative NO_2 distribution maps for the main fire event duration.

2.2.2 Topographic Data and Terrain Derivatives

Given the potential influence of terrain on atmospheric transport processes outlined previously, topographic variables were incorporated into the analysis. These variables were derived from the Shuttle Radar Topography Mission (SRTM) 1 Arc-Second Global DEM, provided by NASA. This dataset offers a spatial resolution of approximately 30 meters and provides sufficient vertical accuracy for regional-scale environmental studies (Farr et al., 2007). Using standard Geographic Information System (GIS) terrain analysis tools (e.g., within QGIS software), three primary topographic parameters were extracted from the DEM (Figure 2):
(i) Elevation (m): Represents the height above mean sea level.

(ii) Slope (°): Quantifies the steepness or the rate of elevation change per unit distance.
(iii) Aspect (°): Indicates the directional orientation of the slope (e.g., North-facing, South-facing), typically measured clockwise in degrees from North (0° to 360°). These terrain derivatives served as key spatial variables for assessing potential terrain-induced variability in NO_2 distribution patterns during the fire event.

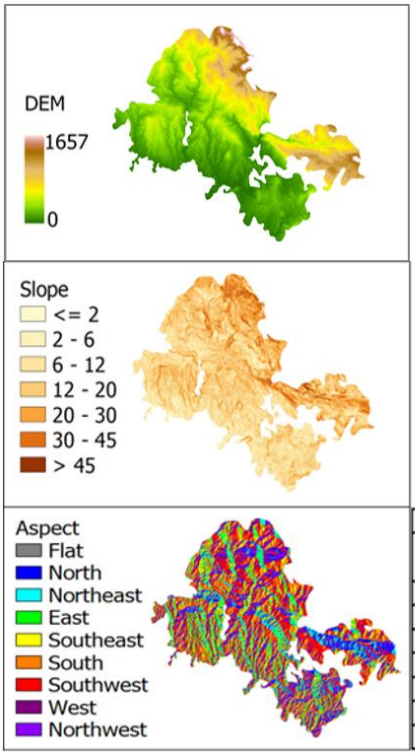

Direction	Degrees (°)
North	0 - 22.5 337.5 - 360
Northeast	22.5 - 67.5
East	67.5 - 112.5
Southeast	112.5 - 157.5
South	157.5 - 202.5
Southwest	202.5 - 247.5
West	247.5 - 292.5
Northwest	292.5 - 337.5

Figure 2. Primary topographic parameters extracted from NASA's 30 m SRTM DEM for the Manavgat fire-affected region: (a) Elevation map. (b) Slope map. (c) Aspect map.

As shown in Figure 2, the study area exhibits a diverse topographic structure characterized by variations in elevation, slope, and aspect. According to the DEM, elevations range from approximately 0 to over 1657 meters. Higher elevations are predominantly concentrated in the northern and northwestern sections of the study area, whereas the southern and southeastern parts are generally characterized by lower elevations approaching sea level. The slope analysis reveals that the majority of the region features moderate slopes, primarily between 6° and 20°. Steeper slopes (greater than 30°) are particularly concentrated in the northern zones, corresponding to higher elevation areas. Flat or gently sloping terrains (≤ 2°) are more commonly observed in the southern and coastal portions of the study area. The aspect map further highlights the directional orientation of the terrain. The study area shows a heterogeneous distribution of aspects; however, south-facing (157.5°–202.5°) and southwest-facing (202.5°–247.5°) slopes are notably prominent. This orientation could influence microclimatic conditions, solar radiation exposure, and consequently, the behavior of pollutant dispersion and vegetation recovery following fire events.

3. Methodology

The analytical methodology employed in this study followed three main stages: (1) Data preparation and preprocessing, (2) Spatial autocorrelation analysis, and (3) Evaluation, as illustrated in the workflow diagram (Figure 3). Each stage is detailed in the subsequent subsections.

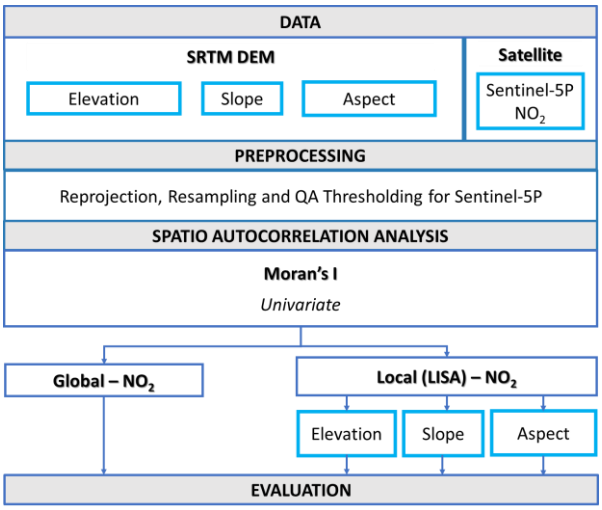

Figure 3. Flowchart of the study.

3.1 Data Preparation and Preprocessing

This initial stage focused on preparing the datasets described in Section 2 (Sentinel-5P NO_2 and SRTM DEM derivatives) for the spatial analysis. Key steps included:

- Processing Sentinel-5P NO_2 data: This was performed within Google Earth Engine (GEE). To ensure data reliability and exclude observations potentially affected by cloud cover or retrieval errors, pixels not meeting the recommended Quality Assurance threshold (QA value > 50%) were filtered out, following standard operational guidelines.
- Temporal consistency: The analysis utilized the temporally organized NO_2 data corresponding to the peak fire activity period (July-August 2021), as mentioned in Section 2.2.1.
- Spatial harmonization: All spatial data layers (NO_2 and DEM derivatives) were projected to a common coordinate system (UTM Zone 36N) to ensure spatial consistency.
- Data Resolution: The analysis used the Sentinel-5P NO_2 data from GEE at its provided spatial resolution of 1.1 km. This dataset was used to create the primary input variable map.

3.2 Spatial Autocorrelation Analysis

To investigate the spatial patterns of NO_2 concentrations during the fire event, spatial autocorrelation analysis was performed using the UV Moran's I statistic. This statistic quantifies the degree to which NO_2 values at nearby locations are similar or dissimilar, indicating clustering, dispersion, or spatial randomness (Moran, 1948; Anselin, 1995). Computations were carried out using the PySAL (Python Spatial Analysis Library) (Rey and Anselin, 2007).

Two forms of UV Moran's I were calculated, as detailed in Table 1:

- Global Moran's I: Provides a single value summarizing the overall degree of spatial autocorrelation across the entire study area.
- Anselin's Local Moran's I (LISA - Local Indicators of Spatial Association): Detects statistically significant

spatial clusters and spatial outliers. It identifies High-High (HH) clusters (areas where high NO_2 concentrations are surrounded by other high values) and Low-Low (LL) clusters (areas where low concentrations are surrounded by low values), as well as spatial outliers, including High-Low (HL - high values surrounded by low values) and Low-High (LH - low values surrounded by high values) patterns.

Statistic	Explanation	Equation
Global Moran's I	Summarizes the overall spatial autocorrelation across the entire study area.	$\frac{n \sum_{i=1}^{n} \sum_{j=1}^{n} w_{ij} (x_i - \bar{x}) (x_j - \bar{x})}{(\sum_{i=1}^{n} \sum_{j=1}^{n} w_{ij}) \sum_{i=1}^{n} (x_i - \bar{x})^2}$
Anselin's Local Moran's I (LISA)	Identifies localized clusters and spatial outliers.	$\frac{n (x_i - \bar{x}) \sum_{j=1}^{n} w_{ij} (x_j - \bar{x})}{\sum_{j=1}^{n} (x_j - \bar{x})^2}$
In both equations, x represents the variable, and $\bar{x}$ denotes its mean. The term x_i signifies the value of the variable at a specific spatial unit (e.g., pixel), while x_j represents the value of at another unit. Here, n refers to the total number of spatial units, and w_{ij} is the row-standardized weight matrix.		

Table 1. UV Moran's I statistics used.

A crucial step in calculating Moran's I is the definition of spatial proximity through a spatial weights matrix (wij). In this study, a first-order Queen contiguity weights matrix was adopted, where adjacent grid cells sharing either an edge or a corner are considered neighbors. To ensure comparability across observations, the weights matrix was row-standardized, assigning equal total influence to each spatial unit.

4. Results

Figure 4 shows dynamic day-to-day variations in the spatial distribution and intensity of NO_2 concentrations from July 28th to August 4th. Starting with low levels across the region on July 28th, a dramatic increase occurred on July 29th, leading to widespread high concentrations (approaching or exceeding 0.0002 mol/m²) primarily across the western and central areas, a pattern which largely persisted through August 1st. A notable shift occurred on August 2nd and 3rd, where the highest NO_2 levels became distinctly localized in the northwestern sector, closely corresponding to the indicated fire activity in that zone, while concentrations elsewhere decreased. By August 4th, a general reduction in NO_2 was evident across the monitored area, with only moderate concentrations remaining in the north-central region. Overall, the highest NO_2 concentrations consistently appeared near the active fire zones, but the specific location and extent of the plume varied significantly daily, underscoring the dynamic influence of fire behavior and likely transport patterns.

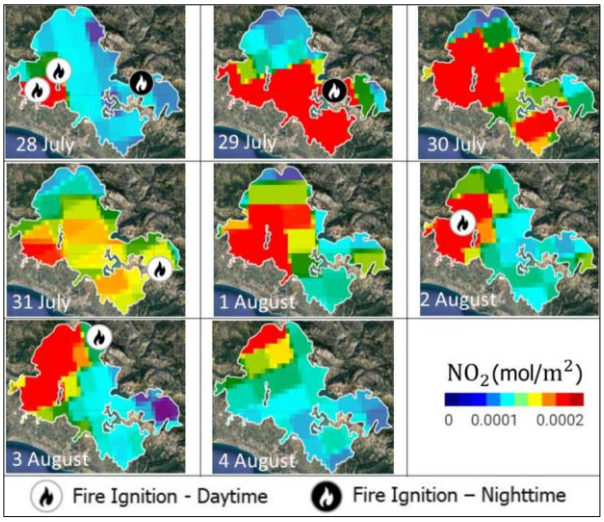

Figure 4. Daily NO_2 concentrations derived from Sentinel-5P satellite data.

As the next step, spatial autocorrelation analysis was conducted by calculating the UV Global Moran's I values for NO_2 concentrations during the study period (Figure 5). The results reveal a strong spatial autocorrelation, with Moran's I values consistently ranging from 0.90 to 0.94 across the entire observation period. While slight variations are observed on different days, the spatial association of NO_2 concentrations remains robust, as evidenced by values consistently exceeding 0.90.

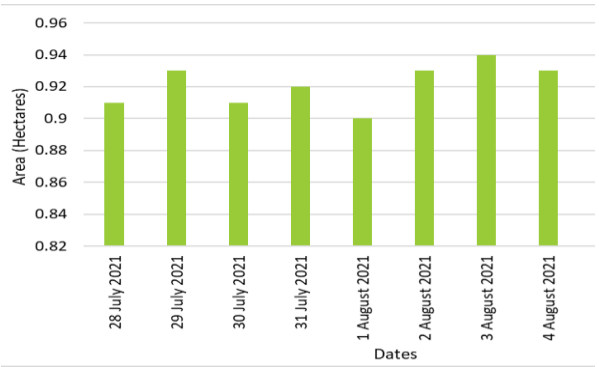

Figure 5. UV Global Moran's I values for NO_2 from 28 July to 4 August 2021.

Following the UV Global Moran's I analysis, which provided an overall indication of spatial autocorrelation across the study area, the UV Local Moran's I was applied to identify specific regions exhibiting significant clusters of high or low NO_2 concentrations (Figure 6). HH clusters were frequently observed in low-lying areas. In contrast, LL clusters were more prevalent in regions farther from the fire fronts or in areas where firefighting interventions may have successfully reduced fire intensity. Furthermore, NO_2 plumes appeared to remain more localized around the most intense combustion zones. The distinct day-to-day fluctuations in NO_2 concentration patterns and associated cluster configurations highlight the dynamic influence of environmental factors—including topography, wind speed and direction, and proximity to active ignition points—on the spatial distribution and temporal evolution of these fire-emitted gases.

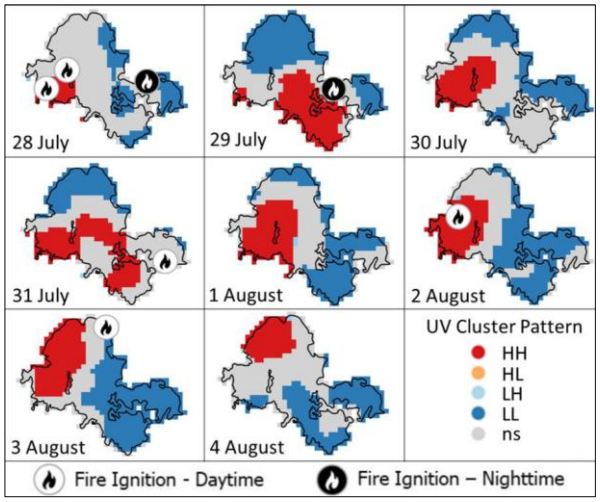

Figure 6. Daily NO_2 cluster patterns calculated using UV Local Moran's I.

As the final step, given that this study focused exclusively on the impact of topography, Figure 7 provides insights into the topographic characteristics associated with statistically significant spatial clustering of NO_2 concentrations, identified as HH and LL clusters based on the UV Local Moran's I analysis, during the period from 28 July to 4 August. The analysis examines the daily distribution of the area (in hectares) covered by these clusters across different elevation (DEM), slope, and aspect categories.

Elevation (DEM): The Local Moran's I clustering reveals that high fire density clusters (HH) predominantly occurred in low-altitude zones (0–500 m), particularly during the early fire days (28–31 July). This suggests a statistically significant spatial concentration of burned areas in lower elevations, possibly valleys or plains (Figure 7a). UV-LL clusters, indicating areas of low NO_2 surrounded by other low values, are also most prevalent in the 0-500m range, particularly peaking later in the period (e.g., August 3rd). However, LL clusters show a more substantial presence in the mid-elevation range (500-1000m) compared to HH clusters, and even some presence at the highest elevations (>1000m). This implies that areas with consistently low NO_2 (relative to their surroundings) occurred across a wider elevation spectrum, potentially representing unburnt areas, regions far from the main plume, or zones where fire activity had diminished or was suppressed.

Slope: Slope-based LISA analysis indicated that HH clusters were mainly concentrated within the 6°–20° slope classes, especially during the days with the most extensive high NO_2 concentrations (July 29-31), confirming the critical role of moderate slopes in facilitating fire expansion through topographically enhanced convection and fuel continuity (Figure 7b). Areas with very gentle slopes (< 6 degrees) and very steep slopes (> 30 degrees) generally host smaller areas of HH clusters. Similarly, UV-LL clusters also peak in the moderate slope categories, notably within the 12-20 degree range (especially prominent around August 3rd), but also significantly in the 6-12 and 20-30 degree ranges. Compared to HH clusters, LL clusters seem slightly more distributed across the slope spectrum, potentially occupying larger areas on both gentler and steeper slopes relative to the HH peaks. This suggests that while fire activity leading to high NO_2 might favor certain moderate slopes, factors leading to low NO_2 concentrations (like distance, wind patterns, or suppression) occur across a somewhat broader range of slope steepness. The wider slope distribution of UV-LL clusters may reflect areas where NO_2 levels remained low due to various factors such as distance from active fire zones, local topographic shielding, or the presence of firebreaks. These patterns could also be influenced by localized atmospheric conditions that limited pollutant accumulation, although further analysis would be needed to confirm such effects.

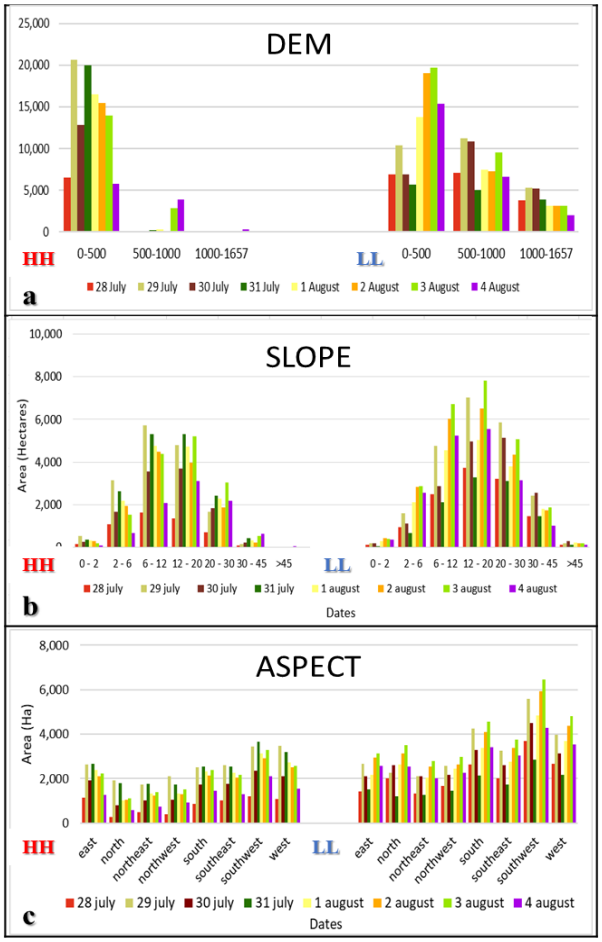

Figure 7. Daily distribution of UV Local Moran's I HH and LL NO_2-based clusters across different elevation, slope and aspect ranges.

Aspect: Compared to elevation and slope, the influence of aspect (slope direction) appears more variable and less decisive, suggesting that atmospheric circulation and fire behavior dynamics exert greater control over the observed spatial clusters (Figure 7c). Both UV-HH and UV-LL clusters are distributed across various aspects on different days. During the peak NO_2 period (July 29-31), HH clusters cover considerable areas on multiple aspects, with perhaps a slight tendency towards East, Southeast, South, Southwest, and West aspects compared to North-facing slopes. It is thought that these aspects receive higher solar radiation, enhancing surface dryness and fuel flammability, thus forming spatially coherent high-risk zones. UV-LL clusters also show a wide distribution, with Southwest and West aspects frequently showing large areas, particularly in the later days (August 2-4). South and Southeast aspects also contribute significantly to LL cluster areas. Although north-facing aspects exhibit relatively smaller clustered areas, both HH and LL clusters are still present. The daily variability suggests that aspect preference is likely strongly modulated by other factors, primarily wind direction

and potentially diurnal heating effects influencing fire spread and plume transport.

5. Conclusion

This study applied spatial autocorrelation analysis, specifically UV Moran's I, to examine satellite-derived NO_2 concentrations during the 2021 Manavgat wildfire. The results provide quantitative insights into how complex topography influenced NO_2 accumulation and dispersion throughout this major fire event, thereby advancing the understanding of pollutant dynamics in fire-prone, topographically heterogeneous regions.

By integrating topographic variables with UV Local Moran's I, the analysis reveals that wildfires and their emissions exhibit significant spatial clustering shaped by terrain characteristics. HH clusters were consistently associated with low elevations (below 500 meters), moderate slopes (6–20 degrees), and sun-exposed aspects—conditions conducive to fire ignition and spread. Although the role of aspect showed greater day-to-day variability, likely driven by wind and fire behavior, the findings emphasize the critical influence of elevation and slope in shaping NO_2 distribution patterns during the fire. These spatial patterns offer valuable guidance for targeted wildfire management and underline the importance of incorporating spatial statistics into fire risk and air quality assessments.

6. Acknowledgements

This study was supported by TÜBİTAK (The Scientific and Technological Research Council of Türkiye) under the 2224-B Domestic Scientific Events Support Program for participation in the GeoVisions 2025 Symposium.

References

Acar, Z., Gonencgil, B., 2023. Forest fires in southern Turkey July-August 2021. *Revista de Climatología*, 23.

Andreae, M.O. and Merlet, P., 2001. Emission of trace gases and aerosols from biomass burning. *Global biogeochemical cycles*, *15*(4), pp.955-966.

Anselin, L., 1995. Local indicators of spatial association—LISA. *Geographical analysis*, 27(2), pp.93-115.

Atalay, H., Sunar, A.F. and Dervisoglu, A., 2025. Spatial Autocorrelation Analysis of CO and NO2 Related to Forest Fire Dynamics. *ISPRS International Journal of Geo-Information*, 14(2), p.65.

D'Andrea, S.D., Ng, J.Y., Kodros, J.K., Atwood, S.A., Wheeler, M.J., Macdonald, A.M., Leaitch, W.R., Pierce, J.R., 2016. Source attribution of aerosol size distributions and model evaluation using Whistler Mountain measurements and GEOS-Chem-TOMAS simulations. *Atmospheric Chemistry and Physics*, 16(1), pp.383-396.

Dillon, G.K., Holden, Z.A., Morgan, P., Crimmins, M.A., Heyerdahl, E.K., Luce, C.H., 2011. Both topography and climate affected forest and woodland burn severity in two regions of the western US, 1984 to 2006. *Ecosphere*, 2(12), pp.1-33.

Farr, T.G., Rosen, P.A., Caro, E., Crippen, R., Duren, R., Hensley, S., Kobrick, M., Paller, M., Rodriguez, E., Roth, L., Seal, D., 2007. The shuttle radar topography mission. *Reviews of Geophysics*, 45(2).

Goodchild MF., 1986. Spatial autocorrelation. Norwich, CN: Geo Books.

Griffin, D., McLinden, C.A., Dammers, E., Adams, C., Stockwell, C., Warneke, C., Bourgeois, I., Peischl, J., Ryerson, T.B., Zarzana, K.J., Rowe, J.P., 2021. Biomass burning nitrogen dioxide emissions derived from space with TROPOMI: Methodology and validation. *Atmospheric Measurement Techniques Discussions*, 2021, pp.1-44.

Griffith, D.A., 2003. Spatial filtering. Springer Berlin Heidelberg.

Jaffe, D.A., Wigder, N.L., 2012. Ozone production from wildfires: A critical review. *Atmospheric Environment*, 51, pp.1-10.

Jaffe, D.A., O'Neill, S.M., Larkin, N.K., Holder, A.L., Peterson, D.L., Halofsky, J.E. and Rappold, A.G., 2020. Wildfire and prescribed burning impacts on air quality in the United States. *Journal of the Air & Waste Management Association*, 70(6), pp.583-615.

Ialongo, I., Virta, H., Eskes, H., Hovila, J., Douros, J., 2020. Comparison of TROPOMI/Sentinel-5 Precursor NO 2 observations with ground-based measurements in Helsinki. *Atmospheric Measurement Techniques*, 13(1), pp.205-218.

Moran, P.A., 1948. The interpretation of statistical maps. Journal of the Royal Statistical Society. Series B (Methodological), 10(2), pp.243-251.

Pausas, J.G., Fernández-Muñoz, S., 2012. Fire regime changes in the Western Mediterranean Basin: from fuel-limited to drought-driven fire regime. *Climatic Change*, 110(1), pp.215-226.

Rey, S. J., Anselin, L., 2007. PySAL: A Python Library of Spatial Analytical Methods, The Review of Regional Studies, 37, 5–27.

Rotach, M.W. and Zardi, D., 2007. On the boundary-layer structure over highly complex terrain: Key findings from MAP. Quarterly Journal of the Royal Meteorological Society: *A journal of the atmospheric sciences, applied meteorology and physical oceanography*, 133(625), pp.937-948.

Soler, M.R., Arasa, R., Merino, M., Olid, M., Ortega, S., 2011. Modelling local sea-breeze flow and associated dispersion patterns over a coastal area in north-east Spain: a case study. *Boundary-layer Meteorology*, 140, pp.37-56.

Val Martin, M., Kahn, R.A., Logan, J.A., Paugam, R., Wooster, M., Ichoku, C., 2012. Space-based observational constraints for 1-D fire smoke plume-rise models. *Journal of Geophysical Research: Atmospheres*, 117(D22).

Veefkind, P., Van Oss, R.F., Eskes, H., Borowiak, A., Dentner, F., Wilson, J., 2007. The applicability of remote sensing in the field of air pollution. Institute for Environment and Sustainability, Italy, 59, pp.1-54.

Veefkind, J.P., Aben, I., McMullan, K., Förster, H., De Vries, J., Otter, G., Claas, J., Eskes, H.J., De Haan, J.F., Kleipool, Q., Van Weele, M., 2012. TROPOMI on the ESA Sentinel-5 Precursor: A GMES mission for global observations of the atmospheric composition for climate, air quality and ozone layer applications. *Remote Sensing of Environment*, 120, pp.70-83.

Wiedinmyer, C., Quayle, B., Geron, C., Belote, A., McKenzie, D., Zhang, X., O'Neill, S. and Wynne, K.K., 2006. Estimating emissions from fires in North America for air quality modeling. *Atmospheric Environment*, 40(19), pp.3419-3432.

Whiteman, C.D., 2000. Mountain meteorology: fundamentals and applications. Oxford University Press.

Zhang, Z., Xu, X., Qiao, L., Gong, D., Kim, S.J., Wang, Y. and Mao, R., 2018. Numerical simulations of the effects of regional topography on haze pollution in Beijing. *Scientific reports*, 8(1), p.5504.